

# Birefringence and quasinormal modes of the Einstein-Euler-Heisenberg black hole

Nora Breton<sup>\*</sup>

*Departamento de Física, CINVESTAV-IPN,  
Apartado Postal 14-740, C.P. 07000, México City, México*

L. A. López<sup>†</sup>

*Área Académica de Matemáticas y Física,  
UAEH, Carretera Pachuca-Tulancingo Km. 4.5,  
C.P. 42184, Mineral de la Reforma, Hidalgo, México*



(Received 24 April 2021; accepted 24 June 2021; published 26 July 2021)

In this contribution we study the birefringence and the quasinormal modes (QNM) in the eikonal approximation of the Einstein-Euler-Heisenberg black hole (EEH-BH). The EEH-BH is an exact solution of the Einstein equations coupled with the Euler-Heisenberg nonlinear electrodynamics. In the Euler-Heisenberg theory the phenomenon of birefringence arises and then there exists two possible light trajectories in the vicinity of the EEH-BH. On the other hand, using the correspondence between the parameters of the unstable null geodesics and the QNM in the eikonal approximation we have determined the QNM of gravitational and electromagnetic perturbations for both the electric and the magnetic EEH-BH and we compared them with their linear counterpart, the Reissner-Nordström black hole. Regarding electromagnetic perturbations we have to consider that there are two effective optical metrics and to each one corresponds one null geodesic that renders two electromagnetic QNMs from the same compact object.

DOI: [10.1103/PhysRevD.104.024064](https://doi.org/10.1103/PhysRevD.104.024064)

## I. INTRODUCTION

These days the existence of black holes (BH) has been widely accepted, or at least the existence of very compact astrophysical objects that resemble several characteristics ascribable to a BH. In most of the observations BHs are accompanied by magnetic fields of varied intensities that go from  $10^{-6}$  Gauss in the centers of galaxies to orders of  $10^{12}$  Gauss for neutron stars [1]. These magnetic fields are of unknown origin, so far; in neutron stars they may have an internal origin. In the case of strong magnetic fields they very likely produce vacuum polarization in their vicinity, then processes like photon splitting, pair conversion or vacuum polarization are expected to occur in the neighborhood of neutron stars [2].

In the presence of intense electromagnetic fields quantum electrodynamics predicts that a vacuum has properties of a material medium as a consequence of the electromagnetic self-interactions. These effects become significant when electromagnetic fields approach the critical strengths,  $E_c \approx 10^{18}$  Volt/m or  $B_c \approx 10^{13}$  Gauss; among them are light-light interaction or electron-positron creation (vacuum polarization). Therefore an electromagnetic (EM) wave

traveling through intense EM fields will change its velocity and the direction of propagation depending on its polarization. This later effect is the birefringence [3–5]. Experimental efforts are currently in progress to observe these nonlinear electrodynamic (NLED) effects in a laboratory; we mention just a few of them, like the detection of vacuum birefringence with intense laser pulses [6–8], or using waveguides [9].

By treating the vacuum as a medium, the Euler-Heisenberg (EH) theory [10,11] predicts rates of nonlinear light interaction processes since it takes into account vacuum polarization to one loop, and is valid for electromagnetic fields that change slowly compared to the inverse electron mass. The EH Lagrangian depends in a nonlinear way on the two Lorentz and gauge invariants,  $F$  and  $G$ ,

$$\mathcal{L}_{\text{EH}}(F, G) = -\frac{F}{4} + \frac{\mu}{4} \left( F^2 + \frac{7}{4} G^2 \right), \quad (1)$$

where  $F = F^{\mu\lambda} F_{\mu\lambda} = 2(B^2 - E^2)$  and  $G = -{}^*F^{\mu\lambda} F_{\mu\lambda} = 4\vec{B} \cdot \vec{E}$ , with  $F_{\mu\lambda}$  being the Faraday tensor, and  ${}^*F_{\mu\nu} = \frac{1}{2\sqrt{-g}} \epsilon_{\mu\nu\rho\sigma} F^{\rho\sigma}$  being its dual, while  $\mu$  is the parameter of the EH theory that in terms of the fine structure constant,  $\alpha$ , is

<sup>\*</sup>nora@fis.cinvestav.mx  
<sup>†</sup>Corresponding author.  
lalopez@uaeh.edu.mx

$$\mu = \frac{2\alpha^2}{45m_e^4}, \quad (2)$$

or in terms of the critical fields is of the order  $\mu \sim \alpha/B_c^2$ . The linear electromagnetic Maxwell theory is recovered if  $\mu = 0$ ; then  $\mathcal{L}_{\text{Maxwell}}(F) = -F/4$ . The Lagrangian in (1) is actually the Euler-Kockel Lagrangian [10], that is the EH Lagrangian expanded up to second-order in  $\alpha$ . Coupling the EH theory with gravitation, BH solutions can be obtained; the static spherically symmetric solution represents a BH with an electric (or magnetic) charge that generates such intense EM fields in which NLED effects arise like the birefringence of light rays. On the other hand, a BH may be characterized by relating its independent parameters to the quasinormal modes (QNM) that result from the response of a test field perturbing the BH spacetime. QNMs have been one of the most useful tools for BH characterization. In the geometric-optics or eikonal approximation the QNM can be determined from the unstable null geodesics that are the orbits attached to the maximum of the effective potential barrier felt by light rays on their interaction with the BH. In 1984 Ferrari and Mashhoon [12] suggested an analytical technique of calculating the QNM in the eikonal limit and later on Cardoso [13] showed the relationship among unstable null geodesics, Lyapunov exponents and the QNM for a stationary spherically symmetric spacetime. The idea basically consists of interpreting the black hole-free oscillations in terms of null particles trapped at the unstable circular orbit and slowly leaking out. The real part of the complex QNM frequencies is determined by the angular velocity at the unstable null geodesic; the imaginary part is related to the instability time scale of the orbit. As compared with the WKB method, calculating the QNM in the eikonal approximation turns out to be good for large angular momentum perturbations in the lowest modes.

Unstable null geodesics derived from the BH metric are followed, in the eikonal limit, by gravitational and massless scalar perturbations. However, electromagnetic perturbations behave differently, as a result of the nonlinear interaction. Light rays do not follow the null geodesics of the background metric, but do follow the null geodesics of an effective optical metric that depends on the nonlinear electromagnetic energy momentum tensor [14,15]. The Einstein-Euler-Heisenberg black hole (EEH-BH) is characterized by a strong field in its vicinity. An EM field of such strength produces birefringence, i.e., two different trajectories for light rays, that are the null geodesics of the effective metrics derived from the study of the propagation of the characteristic surfaces of the EM field [14,15].

In this contribution we determine the two effective metrics whose null geodesics are the light trajectories as well as the QNM in the eikonal approximation arising from perturbing the static EEH-BH. Due to the birefringence effect the QNM of two different frequencies will arise, corresponding to the two different effective optical metrics

emerging due to the NLED interaction of light rays and the strong field background. We determine the unstable circular null orbits that are followed by light rays and then the QNM in the eikonal approximation. We address both the electric and magnetic EEH-BH.

The paper is organized as follows. In the next section a short summary of the EH-NLED and the static spherically symmetric solution of the EEH equations are presented. In Sec. III, we derive the two effective optical metrics that arise in the EH-NLED in both cases, the electric and magnetically charged BH. In Sec. IV we give a brief explanation for determining the QNM in the eikonal limit using the unstable null geodesic and the Lyapunov exponent, as well as give their expressions in terms of the effective potential and the radius of the unstable circular null orbits. In Sec. V we present the explicit expressions for the QNM of the gravitational (or massless scalar) and electromagnetic perturbations, in the eikonal limit and in the spacetime of the EEH-BH; we compare them with the corresponding linear (Maxwell) limit, the Reissner-Nordström black hole (RN-BH). Conclusions are given in Sec. VI.

## II. THE EINSTEIN-EULER-HEISENBERG BLACK HOLE

The four-dimensional action of general relativity coupled to the EH-NLED with Lagrangian  $\mathcal{L}_{\text{EH}}(F, G)$  is

$$S = \frac{1}{4\pi} \int_{M^4} d^4x \sqrt{-g} \left[ \frac{R}{4} - \mathcal{L}_{\text{EH}}(F, G) \right], \quad (3)$$

where  $g$  is the determinant of the metric tensor,  $R$  is the Ricci scalar and  $\mathcal{L}_{\text{EH}}(F, G)$  is the EH Lagrangian in Eq. (1).

Regarding NLEDs there are two possible frameworks [14]. One of them is the usual  $F$ -framework in terms of the electromagnetic field tensor  $F^{\mu\nu}$ . Alternatively, there is the  $P$ -framework with the tensor  $P_{\mu\nu}$  as the main field, defined by

$$P_{\mu\nu} = -(\mathcal{L}_F F_{\mu\nu} + {}^*F_{\mu\nu} \mathcal{L}_G), \quad (4)$$

where the subscript  $X$  in  $\mathcal{L}$  denotes the derivative,  $\mathcal{L}_X = d\mathcal{L}/dX$ . In the Euler-Heisenberg theory,  $P_{\mu\nu}$  takes the form

$$P_{\mu\nu} = (1 - \mu F)F_{\mu\nu} - {}^*F_{\mu\nu} \frac{7\mu}{4}G. \quad (5)$$

The tensor  $P_{\mu\nu}$  corresponds to the electric displacement  $\mathbf{D}$  and the magnetic field  $\mathbf{H}$  while  $F_{\mu\nu}$  corresponds to the magnetic intensity  $\mathbf{B}$  and the electric field  $\mathbf{E}$ , and Eq. (5) is the constitutive relation between  $(\mathbf{D}, \mathbf{H})$  and  $(\mathbf{E}, \mathbf{B})$  in the EH-NLED.

The two NLED frameworks,  $F$  and  $P$ , correspond to the Lagrangian and Hamiltonian treatments, respectively. The

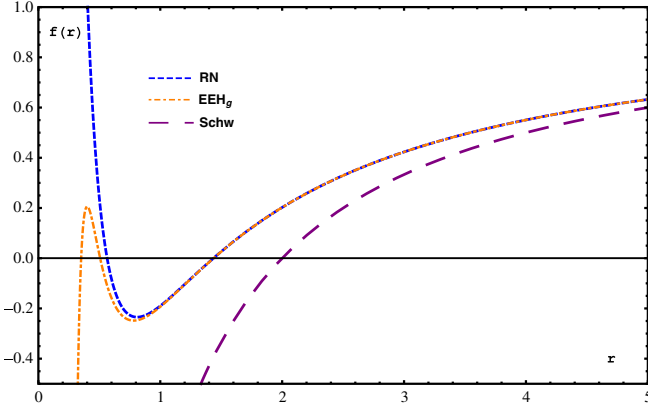


FIG. 1. The behavior of the metric functions  $f(r)$  of the Schwarzschild equation, the electric EEH–BH and the RN BH is shown. Note that the singularity is of opposite sign in the RN and the EEH–BH. The EH parameter  $\mu$  is fixed to  $\mu = 0.107$ ,  $M = 1$  and  $Q_e = 0.9$ .

two invariants associated with the P framework,  $s$  and  $t$ , are defined as

$$s = -\frac{1}{4}P_{\mu\nu}P^{\mu\nu}, \quad t = -\frac{1}{4}P_{\mu\nu}{}^*P^{\mu\nu}, \quad (6)$$

with  ${}^*P_{\mu\nu} = \frac{1}{2\sqrt{-g}}\epsilon_{\mu\nu\rho\sigma}P^{\rho\sigma}$  being the dual tensor to  $P_{\mu\nu}$ . The Legendre transformation of  $\mathcal{L}$  defines the Hamiltonian or structural function  $\mathcal{H}$ ,

$$\mathcal{H}(s, t) = -\frac{1}{2}P^{\mu\nu}F_{\mu\nu} - \mathcal{L}. \quad (7)$$

Neglecting the second- and higher-order terms in  $\mu$ , the structural function for the EH theory takes the form [16]

$$\mathcal{H}(s, t) = s - 4\mu\left(s^2 + \frac{7\mu}{4}t^2\right). \quad (8)$$

The EM and gravitational field equations are then

$$\nabla_{\mu}P^{\mu\nu} = 0, \quad G_{\mu\nu} + \Lambda g_{\mu\nu} = 8\pi T_{\mu\nu}. \quad (9)$$

The energy momentum tensor  $T_{\mu\nu}$  for the EH theory in the P framework is given by

$$T_{\mu\nu} = \frac{1}{4\pi} \left\{ (1 - \mu s)P_{\mu}^{\beta}P_{\nu\beta} + g_{\mu\nu} \left( s - \frac{\mu}{2} \left[ 3s^2 + \frac{7}{4}t^2 \right] \right) \right\}. \quad (10)$$

In the next subsections we present the static spherically symmetric solution of the EEH equations which are, in both cases, electric and magnetically charged.

### A. Electrically charged EEH–BH solution

The solution to Eq. (9) for a static spherically symmetric (SSS) metric of the form

$$ds^2 = -f(r)dt^2 + f(r)^{-1}dr^2 + r^2(d\theta^2 + \sin^2\theta d\phi^2), \quad (11)$$

with  $f(r) = 1 - 2m(r)/r$ , was derived in [17] using the NLED P-framework [14] (see also [16]). The metric function for the electric case is given by

$$f(r) = 1 - \frac{2M}{r} + \frac{Q_e^2}{r^2} - \frac{\mu Q_e^4}{20r^6}, \quad (12)$$

where  $M$  is the mass of the BH,  $Q_e$  is its electric charge and  $\mu$  is the EH parameter. The Reissner-Nordström (RN) solution is the SSS solution to the coupled Einstein-Maxwell equations; which in this case is recovered from (12) by making  $\mu = 0$ .

In [16] the interpretation of the EH-effect is emphasized as a charge screening due to the vacuum polarization effect and it is proved that, for a fixed charge, the EH-BH is more gravitationally attractive than the RN-BH, because the electrostatic energy is smaller than the RN. The screening effect is clear by writing the metric function  $g_{tt}$  in Eq. (12) as

$$f(r) = 1 - \frac{2M}{r} + \frac{Q_e^2}{r^2} \left\{ 1 - \frac{\mu Q_e^2}{20r^4} \right\}. \quad (13)$$

In general the behavior of  $f(r)$  is Schwarzschild-like if compared with other NLED-BHs that have an RN behavior but with a screened charge (for instance Born-Infeld BH [18,19]). In Fig. 1 we show the metric functions of the Schwarzschild, Reissner-Nordström and Einstein-Euler-Heisenberg equations; the RN is the most compact object, while the EEH-BH event horizon is located between the former. For the EEH–BH the singularity remains at  $r = 0$  and is stronger and of the opposite sign than in the RN. The equation that determines the horizons at  $r_+$ ,  $f(r_+) = 0$  is a six degree polynomial equation,

$$r_+^6 - 2r_+^5 + Q_e^2 r_+^4 - \frac{\mu Q_e^4}{20} = 0; \quad (14)$$

the previous equation has been written in terms of  $r \mapsto r/M$  and the dimensionless parameters,  $Q_e \mapsto Q_e/M$  and  $\mu \mapsto \mu/M^2$ . The number of horizons may vary from three to one. By applying the method described in [20], we determine the range of values for  $Q_e$  and  $\mu$ , so that the line element of the Euler-Heisenberg in the electric case (12) represents a black hole or an extreme black hole. For  $\mu/M^2 \leq 50/81$  and  $Q_e^2/M^2 \leq 25/24$  Eq. (14) may have three real positive roots (one outer horizon and two inner horizons); the extreme case can be obtained from the conditions  $f(r) = 0$  and  $df(r)/dr = 0$ , that amounts to the EH parameter  $\mu$  being

$$\mu_{\text{ext}} = \frac{5^5(1 \pm \sqrt{1 - 24Q_e^2/25})^4(6Q_e^2 - 5(1 \mp \sqrt{1 - 24Q_e^2/25}))}{18^3 Q_e^4}. \quad (15)$$

Note that while the charge of the RN-BH is constrained to  $Q^2 \leq M^2$ , and due to the screening charge effect this bound is stretched to  $Q^2 \leq (1.04)M^2$  in the EEH-BH.

In the P-framework the purely electric field is given by the antisymmetric tensor  $P_{\mu\nu}$  that for an SSS metric has the form

$$P_{\mu\nu} = \frac{Q_e}{r^2}(\delta_\mu^1 \delta_\nu^0 - \delta_\mu^0 \delta_\nu^1); \quad (16)$$

then the EM invariants,  $s$  and  $t$  from Eq. (6), are given by

$$s = \frac{Q_e^2}{2r^4}, \quad t = 0. \quad (17)$$

The tensor  $P_{\mu\nu}$  is related to the Faraday tensor  $F_{\mu\nu}$  by the constitutive or material relations

$$F_{\mu\nu} = \left(1 - \mu s - \frac{7\mu}{4} t\right) P_{\mu\nu}; \quad (18)$$

therefore in this case (electrical) the nonvanishing component of the Faraday tensor is

$$F_{01} = \left(1 - \frac{\mu P_{01}^2}{2}\right) P_{01}, \quad (19)$$

where  $P_{01}$  is given in Eq. (16). In [21] the electric case in the NLED  $F$ -framework is treated; see also [22]. Recently, a stationary EEH solution [23] has been derived from the electric static EEH solution.

### B. Magnetically charged EEH–BH solution

The SSS solution of the magnetically charged EEH-BH has the same metric component  $g_{tt} = f(r)$  in Eq. (12) but replaces the electric charge with a magnetic one,  $Q_e \mapsto Q_m$ . The magnetic case is more conveniently obtained in the F-framework of NLEDs with the magnetic field given by

$$F_{\mu\nu} = Q_m \sin \theta (\delta_\mu^3 \delta_\nu^2 - \delta_\mu^2 \delta_\nu^3), \quad (20)$$

while the invariants in this case are  $F = 2Q_m^2/r^4$  and  $G = 0$ . The magnetic EEH–BH horizons also have been analyzed in [24] and [16].

### III. EFFECTIVE OPTICAL METRICS OF THE EEH–BH

The theory defined by the Lagrangian  $\mathcal{L}_{\text{EH}}(F, G)$  (1) admits the phenomenon of birefringence. By this we mean that light rays with different polarizations do follow distinct trajectories. These trajectories are determined by the null geodesics of an effective optical metric  $\gamma^{\mu\nu}$  (or pseudo-metric) that depends on the matter tensor. The effective metric can be calculated from the study of the characteristic surfaces or the propagation of discontinuities of the electromagnetic field [14], such that  $\gamma^{\mu\nu} \kappa_\mu \kappa_\nu = 0$  with  $\kappa_\nu$  being a null vector normal to the wavefront of the propagating electromagnetic discontinuities (see also [25,26]). In this treatment, that is equivalent to the *soft photon approximation* [27,28], a system of coupled equations for the effective optical metrics is derived in [15]; in the EH case, in which  $\mathcal{L}_{FG} = 0$ , the system can be decoupled into two effective metrics,  $\gamma^{(i)\mu\nu}$  and  $i = 1, 2$ , given by

$$\begin{aligned} \gamma^{(1)\mu\nu} &= (\mathcal{L}_F - 2\mathcal{L}_{GG}F)g^{\mu\nu} - 4\mathcal{L}_{GG}F_{,\lambda}^{\mu} F^{\lambda\nu}, \\ \gamma^{(2)\mu\nu} &= \mathcal{L}_F g^{\mu\nu} - 4\mathcal{L}_{FF}F_{,\lambda}^{\mu} F^{\lambda\nu}, \end{aligned} \quad (21)$$

where  $g^{\mu\nu}$  is the background metric, that in our case of interest is the EEH–BH metric, Eq. (11) with Eq. (12). Another NLED that exhibits birefringence was explored in [29].

#### A. Effective optical metrics for the electric EEH–BH

Given an SSS metric  $g_{\mu\nu}$ , of the form (11), and the electromagnetic field in Eq. (19), the two effective metrics of Eq. (21) explicitly become

$$\gamma^{(1)\mu\nu} = \left(-\frac{1}{4} + \frac{5}{2}\mu P_{01}^2\right)g^{\mu\nu} - \frac{7}{2}\mu F_{,\lambda}^{\mu} F^{\lambda\nu}, \quad (22)$$

$$\gamma^{(2)\mu\nu} = \left(-\frac{1}{4} - \mu P_{01}^2\right)g^{\mu\nu} - 2\mu F_{,\lambda}^{\mu} F^{\lambda\nu}, \quad (23)$$

where we have substituted the EM invariant  $F$  given by

$$F = -2F_{01}^2 = -2(1 - aP_{01}^2)P_{01}^2, \quad (24)$$

where  $P_{01}$  is given by Eq. (16) and we have neglected terms of  $\mathcal{O}(\mu^2)$ , to be consistent with the EH Lagrangian that is valid up to  $\mu$ -order. The effective metrics (22) and (23), up to a conformal factor that leave null geodesics invariant, can be comprised in the formula for the line element,

$$\gamma_{\mu\nu}^{(i)} dx^\mu dx^\nu = \frac{1}{G_i^e(r)} \left( -f(r) dt^2 + \frac{dr^2}{f(r)} \right) + r^2 d\Omega^2, \quad (25)$$

$$i = 1, 2,$$

with

$$G_1^e(r) = 1 - \left( \frac{4\mathcal{L}_{GG}(F_{10})^2}{\mathcal{L}_F - 2\mathcal{L}_{GG}F} \right) = 1 + \mu \frac{14(F_{01})^2}{1 + 5\mu F}, \quad (26)$$

$$G_2^e(r) = 1 - \left( \frac{4\mathcal{L}_{FF}(F_{10})^2}{\mathcal{L}_F} \right) = 1 + \mu \frac{8(F_{01})^2}{1 - 2\mu F}. \quad (27)$$

The factors  $G_i^e$  become 1 in the linear case, where there is no birefringence at all. Notice that the terms responsible for birefringence depend on  $\mathcal{L}_{GG}$  or  $\mathcal{L}_{FF}$ , therefore, birefringence arises only from NLED Lagrangians depending on the EM invariants in a nonlinear way. In other words, if  $\mathcal{L}_{GG} = 0$  or  $\mathcal{L}_{FF} = 0$ , there is not birefringence. In the previous expressions we must keep terms up to first-order in  $\mu$  (second-order in  $\alpha$ ), obtaining then

$$G_1^e(r) = 1 + 14\mu \frac{Q_e^2}{r^4}, \quad G_2^e(r) = 1 + 8\mu \frac{Q_e^2}{r^4}. \quad (28)$$

In Fig. 2 the metric functions  $g_{tt} = f(r)$  of the Reissner-Nordström and Einstein-Euler-Heisenberg background metric ( $\text{EEH}_g$ ) are compared, including as well the two effective optical metrics of the electric EEH-BH ( $\text{EEH}_1$  and  $\text{EEH}_2$ ).

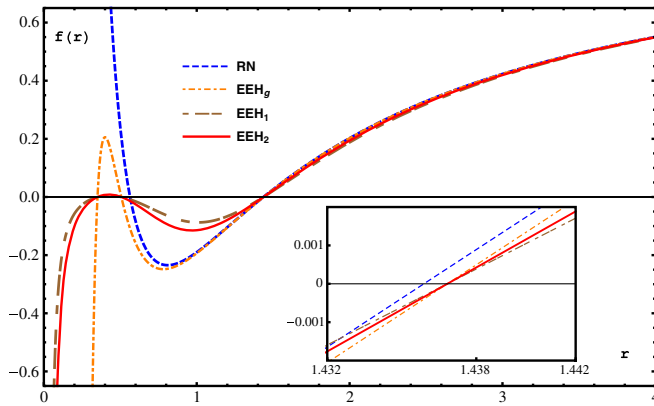


FIG. 2. The behavior of the metric functions  $f(r)$  of the electric EEH-BH ( $\text{EEH}_g$ ) and RN-BH are shown as well as those corresponding to the two optical metrics, denoted in the plot as  $\text{EEH}_1$  and  $\text{EEH}_2$  (note in the small box that the horizon of the EEH metrics is one and the same, while the RN horizon is the shortest). The EH parameter  $\mu$  is fixed to  $\mu = 0.107$ ,  $M = 1$  and  $Q_e = 0.9$ .

## B. Effective optical metrics for the magnetic EEH-BH

For the magnetic case, the electromagnetic field is given by Eq. (20), and there is birefringence as well. The effective optical metrics from Eq. (21) are given by

$$\gamma_{\mu\nu}^{(i)} dx^\mu dx^\nu = G_i^m(r) \left( -f(r) dt^2 + \frac{dr^2}{f(r)} \right) + r^2 d\Omega^2, \quad (29)$$

$$i = 1, 2,$$

with

$$G_1^m(r) = 1 - 12\mu \frac{Q_m^2}{r^4}, \quad G_2^m(r) = 1 - 4\mu \frac{Q_m^2}{r^4}, \quad (30)$$

where  $Q_m$  is the magnetic charge and we have only kept terms up to  $\mathcal{O}(\mu)$ .

## IV. THE QNM AND UNSTABLE NULL GEODESICS IN SSS SPACES

The connection between the QNM and bound states of the inverted black hole effective potential was pointed out in [12]. In [13] it was shown that, in the eikonal limit, the QNMs of black holes are determined by the parameters of the unstable circular null geodesics. The real part ( $\omega_r$ ) of the complex QNM frequencies is determined by the angular velocity  $\Omega_c$  at the unstable null geodesics, while the imaginary part ( $\omega_{\text{im}}$ ), that is related to the instability time scale of the orbit (relaxation time), is related to the Lyapunov principal exponent  $\lambda$ . The QNM  $\omega_{\text{QNM}}$  are given in the eikonal limit, by

$$\omega_{\text{QNM}} = \omega_r - i\omega_{\text{im}} = \Omega_c l - l \left( n + \frac{1}{2} \right) |\lambda|, \quad (31)$$

where  $n$  is the overtone number and  $l$  is the angular momentum of the perturbation. The Lyapunov exponents are a measurement of the average rate at which nearby trajectories converge or diverge in the phase-space. A positive Lyapunov exponent indicates a divergence between nearby trajectories, i.e., a high sensitivity to initial conditions.

In the case of stationary, spherically symmetric spacetimes it turns out that  $\lambda$  can be expressed as the second derivative of the effective potential evaluated at the radius of the unstable circular null orbit. From the equations of motion and using the definition  $i^2 + V(r) = 0$ , where  $V(r)$  is the effective potential for radial motion, circular geodesics are determined from the conditions  $V(r_c) = V'(r_c) = 0$  where  $r_c$  is the radius of the circular orbit. The Lyapunov exponent in terms of the second derivative of the effective potential is given by

$$\lambda = \sqrt{\frac{-V''}{2i^2}}, \quad (32)$$

where  $t$  is the time coordinate; a dot denotes the derivative with respect to an affine parameter of the geodesic while prime stands for the derivative with respect to  $r$ , while the orbital angular velocity  $\Omega_c$  is given by

$$\Omega_c = \frac{d\varphi}{dt} = \frac{\dot{\varphi}}{\dot{t}}. \quad (33)$$

For our purpose both expressions should be evaluated at  $r_c$ , the radius of the unstable circular null orbit, denoted by the “ $c$ ” subscript; that is the orbit with an impact parameter  $b = L/E$  and with  $V''(r_c) < 0$ .

For an SSS metric of the form seen in Eq. (11), the energy  $E$  and the angular momentum  $L$  of a test particle are conserved quantities,

$$f(r)\dot{t} = E = \text{const}, \quad r^2\dot{\varphi} = L = \text{const}. \quad (34)$$

For equatorial orbits, from the equation of radial motion,  $\dot{r}^2 + V(r) = 0$ , in the SSS spacetime, the effective potential is given by

$$V(r) = E^2 \left( \frac{f(r)L^2}{r^2 E^2} - 1 \right), \quad (35)$$

that for the EEH-BH amounts to

$$V(r)^{\text{EH}} = E^2 \left( \frac{L^2}{r^2 E^2} \left[ 1 - \frac{2M}{r} + \frac{Q^2}{r^2} \left( 1 - \mu \frac{Q^2}{20r^4} \right) \right] - 1 \right). \quad (36)$$

Displayed in Fig. 3 are the effective potentials felt by massless test particles in the electric EEH–BH (denoted by  $\text{EEH}_g$ ) and the RN–BH. Shown as well are the effective potentials for the photons with different polarizations, denoted as  $\text{EEH}_1$  and  $\text{EEH}_2$ .

The Lyapunov exponent from (32), related to the imaginary part of the QNM by  $\omega_{\text{im}} = (n + 1/2)|\lambda|$ , is given by

$$\lambda^2 = \frac{f}{2r^2} [2f - r^2 f'']|_{r_c}, \quad (37)$$

while the orbital angular velocity, that is proportional to the QNM real part  $\omega_r = \Omega_c l$ , is given by

$$\Omega_c = \left( \frac{L f}{E r^2} \right) \Big|_{r_c} = \sqrt{\frac{f}{r^2}} \Big|_{r_c}; \quad (38)$$

in the previous expressions we have incorporated the conditions for a circular orbit,  $V(r_c) = 0$  and  $V'(r_c) = 0$ . These conditions amount, respectively, to

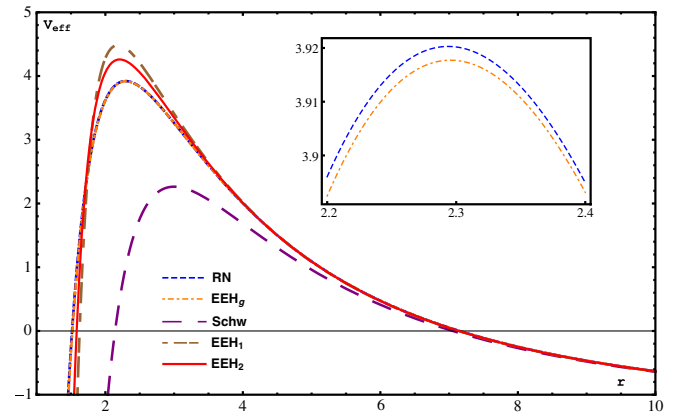


FIG. 3. The behavior of the effective potentials felt by massless test particles in the electric EEH–BH and RN–BH is shown as well as the effective potentials for the photons with different polarizations, denoted as  $\text{EEH}_1$  and  $\text{EEH}_2$ ; these are higher than the other potentials. The Schwarzschild potential is the lowest one; the one felt by gravitons (massless test particles, denoted by  $\text{EEH}_g$ ) is very close to the RN. In the small box the difference is shown. These are the potentials used for the calculations of the unstable null orbits from which we extract the QNM in the eikonal approximation. In this plot  $L = 10$ ,  $E = 1.2$ ,  $M = 1$  and the BH parameters are fixed to  $\mu = 0.6$ ,  $Q_e = 0.9$ .

$$\frac{E^2}{L^2} = \frac{f}{r^2} \Big|_{r_c}, \quad (2f - r f')|_{r_c} = 0. \quad (39)$$

The expressions for the QNM in the case of an NLED Lagrangian  $\mathcal{L}(F)$  that depends only on the invariant  $F$  were derived in [30]. At this point it is worth it to mention that in [31] the validity of the correspondence between the QNM in the eikonal approximation and the unstable null geodesics was analyzed, finding that this correspondence does not hold for the Einstein-Lovelock theories concretely, in the case of the Einstein-Gauss-Bonnet BH. On the other hand the convergence of the QNM, calculated numerically, to the eikonal approximation for an NLED deviation from Maxwell theory was tested in [32].

In the following Sec. V the effective potentials and the corresponding QNM expressions will be written for the SSS solution of the Einstein equations coupled to the EH Lagrangian  $\mathcal{L}_{\text{EH}}(F, G)$  [Eq. (1)].

## V. THE QNM OF THE EEH–BH IN THE EIKONAL APPROXIMATION

In the eikonal regime, scalar and gravitational perturbations behave similarly, following the null geodesics of the background spacetime. In the case of the EEH-BH, the effective potential felt by the massless particles (not photons) is the one in Eq. (36). While EM perturbations of NLED spacetimes do follow the null geodesics of the effective optical metric, EEH-BH follows two different null geodesics, given by Eq. (25) for the electric EEH-BH;

while the two effective optical metrics given by Eq. (29) correspond to the magnetic EEH-BH. The effective potentials are shown in Fig. 3 for the electric EEH-BH (denoted by  $EEH_g$ ) and the RN-BH, as well as the effective potentials for the EM perturbations, denoted as  $EEH_1$  and  $EEH_2$ .

In what follows we address the perturbations in the eikonal limit. First of all in subsection A we describe the perturbations to the SSS solution of the Einstein-Maxwell equations, the RN-BH, whose null geodesics are determined from the metric given by Eqs. (11) and (12) switching off the EH parameter,  $\mu = 0$ . It is well known that the EM perturbations of the electrically and magnetically charged RN-BH are isospectral, however this is not the case for the NLED-BH; this issue has been investigated for instance in [32] regarding parity splitting. The following subsection B describes gravitational (or scalar) perturbations of the EEH-BH, which are determined from the null geodesics of the background metric given by Eqs. (11) and (12) for the electric case; gravitational perturbations for the magnetically charged EEH-BH obey the same equations, but just change  $Q_e \mapsto Q_m$ .

Subsection C is devoted to the electromagnetic perturbations. In this case polarization of the perturbations define which one of the two effective optical metrics governs the light trajectory in the vicinity of the EEH-BH; the effective optical metrics are given by Eq. (25) for the electric case and by Eq. (29) for the magnetically charged EEH-BH. With respect to the perturbations of the NLED-BH, we can mention; in [33] solutions of the coupled Einstein equations with an NLED with  $\mathcal{L}(F)$  are studied; axial electromagnetic perturbations were derived for the regular NLED-BH with the correct weak field limit (Maxwell), while the corresponding polar electromagnetic perturbations were analyzed in [34].

In subsection D the relaxation times are discussed and in subsection E the temporal evolution of the perturbations is discussed.

### A. The QNM of the Reissner-Nordström black hole

The RN is the SSS solution to the Einstein gravity coupled to Maxwell electromagnetism with the Lagrangian  $\mathcal{L} = -F/4$ ,  $\mathcal{L}_F = -1/4$  and  $\mathcal{L}_{FF} = 0$ . In the eikonal limit, both gravitational and electromagnetic perturbations do follow null geodesics of the RN metric. In the RN-BH case, the metric function  $f(r)$  in the line element (11) is given by Eq. (12) with  $\mu = 0$ . The circular null orbit radius  $r_c$  (also known as the radius of the light ring) is calculated from (39), that in the RN case amounts to the quadratic polynomial equation and solution given, respectively, by

$$r_c^2 - 3r_c + 2Q^2 = 0, \quad r_c = \frac{3}{2} \left( 1 + \sqrt{1 - 8Q^2/9} \right), \quad (40)$$

where we have used a dimensionless coordinate  $r \mapsto r/M$  and the dimensionless parameter,  $Q \mapsto Q/M$ . In the eikonal approximation, the QNMs are given by (31) with  $\lambda$  and  $\Omega_c$  calculated as in (37) and (38), respectively, as

$$M^2 \lambda^2 = \frac{1}{r_c^6} [r_c^2 - 2Q^2][Q^2 + r_c^2 - 2r_c],$$

$$M^2 \Omega_c^2 = \frac{1}{r_c^4} [Q^2 + r_c^2 - 2r_c], \quad (41)$$

that, by substituting  $r_c$  from (40), gives

$$M^2 \lambda^2 = \frac{4\sqrt{1 - 8Q^2/9}(1 + 3\sqrt{1 - 8Q^2/9})}{3^3(1 + \sqrt{1 - 8Q^2/9})^4},$$

$$M^2 \Omega_c^2 = \frac{2(1 + 3\sqrt{1 - 8Q^2/9})}{27(1 + \sqrt{1 - 8Q^2/9})^3}. \quad (42)$$

These are the expressions for  $\lambda$  and  $\Omega_c$  for the RN-BH that we will compare with the ones for the EEH-BH to find the amount of departure of the EEH-BH expressions from the linear (Maxwell) case. For the RN-BH, analytic solutions can be found all the way through, however in the EEH case no analytic  $r_c$  solutions were determined.

### B. EEH-BH gravitational (or scalar) perturbations in the eikonal approximation

Gravitational as well as massless scalar perturbations in the eikonal limit obey the null geodesics of the background EEH-BH metric given by Eqs. (11) and (12) for the electric case. Those perturbations for the magnetically charged EEH-BH obey the same equations, just changing  $Q_e \mapsto Q_m$ . The radii of the unstable circular null geodesics are given by Eq. (39) with  $f(r)$  given by (12); these are the positive roots that are larger than the horizon radius of

$$r_c^6 - 3Mr_c^5 + 2Q_e^2 r_c^4 - \mu \frac{Q_e^4}{5} = 0. \quad (43)$$

The radii  $r_c$  of the massless particle unstable null orbits are shown in comparison with the RN one and also corresponding to photons in the vicinity of the EEH-BH in Fig. 4. The QNMs are given by (31) with  $\lambda$  and  $\Omega_c$  calculated as in (37) and (38), respectively, using  $f(r) = 1 - 2M/r + Q^2/r^2 - \mu Q^4/(20r^6)$ . The gravitational QNMs (denoted as  $EEH_g$ ) are compared with the electromagnetic EEH-BH and RN QNM in Figs. 5–7. The difference between the gravitational perturbations and the RN ones is very tiny, and is illustrated in the small boxes.

### C. Electromagnetic perturbations of the EEH-BH QNM in the eikonal approximation

The effective potential for a test photon with impact parameter  $b = L/E$  in the neighborhood of the EEH-BH, from  $i^2 + V(r) = 0$ , is given by

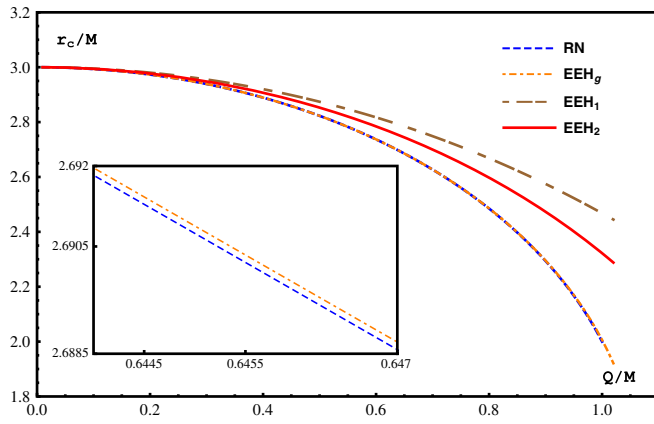


FIG. 4. The behavior of the null circular orbit radii as a function of  $Q/M$  is shown for the electric EEH–BH and RN–BH; the distinction between the RN and EEH<sub>g</sub> is shown in the small box and the relative magnitudes of the radii are  $r_c^{\text{RN}} < r_c^{\text{EEH}_g} < r_c^{\text{EEH}_2} < r_c^{\text{EEH}_1} < r_c^{\text{Schw}} = 3M$ . The EH parameter  $\mu$  is fixed to  $\mu/M^2 = 0.5$ .  $\mu = 0$  is for the RN. The departure point of the curves in the vertical axis corresponds to  $r_c^{\text{Schw}} = 3M$  that is the largest photosphere.

$$V_i(r) = E^2 \left( \frac{G_i^e}{G_i^m} \right)^2 \left( b^2 \frac{G_i^m f(r)}{G_i^e r^2} - 1 \right), \quad (44)$$

where  $G_i^e$  and  $G_i^m$  [given by Eqs. (28) or (30), respectively] are the electric and magnetic factors. In the purely electric EEH–BH  $G_i^m = 1$  and in the purely magnetic case  $G_i^e = 1$ ; in the RN case ( $\mu = 0$ )  $G_i^e = G_i^m = 1$ . The conditions  $V_i(r) = 0$  and  $V_i'(r) = 0$  render the equations to determine the radius of the unstable circular null orbits,  $r_{ic}$ ,

$$\left( \frac{f'}{f} - \frac{2}{r} \right) \Big|_{r_{ic}} = \left( \frac{G_i^e}{G_i^m} \right)' \left( \frac{G_i^m}{G_i^e} \right) \Big|_{r_{ic}}. \quad (45)$$

The corresponding solution should be greater than the horizon radius,  $r_{ic} > r_+$ . The additional condition that defines the sphere of the unstable null photon geodesics is  $V''(r_c) < 0$ . This radius is also known as the radius of the photosphere, that for a Schwarzschild BH is  $r_c = 3M$ .

The imaginary part of the QNM is  $\omega_{\text{im}}^i = (n + 1/2) |\lambda|$ ,  $i = 1, 2$ , where the Lyapunov exponent  $\lambda$  in the EEH–BH case is given by

$$\lambda_i^2 = \frac{-V''_i}{2i^2} = \frac{fr^2}{2} \left( \frac{f}{r^2} \left( \frac{G_i^e}{G_i^m} \right)'' \left( \frac{G_i^m}{G_i^e} \right) - \left( \frac{f}{r^2} \right)'' \right) \Big|_{r_{ic}}, \quad (46)$$

$i = 1, 2.$

The real part of the QNM is  $\omega_r = l\Omega_c$ , with the angular velocity from Eq. (38) given by

$$\Omega_c^{(i)} = \sqrt{\frac{G_i^m f(r)}{G_i^e r^2}} \Big|_{r_{ic}} \quad i = 1, 2. \quad (47)$$

Equations (46) and (47), the EEH–BH versions of (37) and (38), determine the quasinormal frequencies, the imaginary and real parts, respectively, of the EM perturbations to the EEH–BH in the eikonal approximation. As a reference, an  $\mathcal{L}(F)$  NLED–BH whose gravitational (scalar) perturbations are always oscillating with bigger real frequencies than the Schwarzschild one,  $\omega_r(Q \neq 0) > \omega_r^{\text{Schw}}(Q = 0)$ , is studied in [35]; the same qualitative behavior we obtain for the EEH–BH oscillations. Moreover, for all of the EEH–BH perturbations the angular velocity,  $\Omega_c$ , is smaller than the one of the RN–BH, such that  $\omega_r^{\text{Schw}} < \omega_r^{\text{EEH}_1} < \omega_r^{\text{EEH}_2} < \omega_r^{\text{EEH}_g} < \omega_r^{\text{RN}}$ .

In what follows the EEH–BH QNMs are given explicitly for the electric case and are compared with those corresponding to perturbations coming from the linear electromagnetic RN–BH, given in subsection A; the comparison is done with the EEH–BH gravitational perturbations given in subsection B as well. Only the fundamental frequency  $n = 0$  is considered; that is, the least damped mode. Since we restrict to the electric case in this subsection we consider  $G_i^m = 1$ . For the analysis of the EEH–BH QNMs, we consider the dimensionless parameters as in (14). The circular null orbit radii  $r_{ic}$  are obtained from (45), that in the electric EEH–BH case are the roots of

$$5r_{ic}^4 [2Q_e^2 + r_{ic}(r_{ic} - 3)] - \mu Q_e^2 [Q_e^2 + 5a_i r_{ic}(r_{ic} - 1)] = 0, \quad (48)$$

where  $a_1 = 7$  and  $a_2 = 4$ . The analysis of the roots  $r_{1c}$  and  $r_{2c}$  of Eq. (48) is performed numerically in the ranges of  $Q_e$  and  $\mu$  where the EEH solution (12) represents a black hole. Shown in Fig. 4 is the tendency of the roots of Eq. (48), in the case of the EEH–BH, and Eq. (40), for the RN, as a function of  $Q_e/M$ . The null orbit radii  $r_{ic}$  for the EEH–BH approach the corresponding RN for small  $Q_e$ .  $Q_e = 0$  corresponds to the Schwarzschild photosphere,  $r_c^{\text{Schw}} = 3M$ . Increasing the charge makes  $r_c$  decrease, such that the relative magnitudes of the radii are  $r_c^{\text{RN}} < r_c^{\text{EEH}_g} < r_c^{\text{EEH}_2} < r_c^{\text{EEH}_1} < r_c^{\text{Schw}}$ . In this respect the NLED–BH does not have a generic behavior; see for instance the Maxwellian case studied in [35] where the effect in the unstable circular null orbits, for fixed charge, is to shorten the radius  $r_c$  compared with the one of the RN–BH. While for the EEH–BH the screening of the charge has the opposite effect, enlarging the radii of the unstable circular null orbits as compared with those corresponding to the RN–BH, for the same charge.

The QNM imaginary part of the EM perturbations,  $\omega_{\text{im}}^i = (n + 1/2) |\lambda|$ ,  $i = 1, 2$ , is calculated with the Lyapunov exponents  $\lambda_i$ , from Eq. (46), and is given by

$$\begin{aligned}
 M^2 \lambda_i^2 = & \frac{1}{r^6} [r^2 - 2Q_e^2][Q_e^2 + r(r-2)] \\
 & - \frac{\mu Q_e^2}{20r^{10}} [Q_e^2(19r^2 - 40r + 22Q_e^2) \\
 & + 40a_i [Q_e^2 + r(r-2)]^2] \Big|_{r_{ic}}, \quad (49)
 \end{aligned}$$

where  $a_1 = 7$  and  $a_2 = 4$ . In the previous expressions we only kept terms up to  $\mathcal{O}(\mu)$  to be consistent with the EH theory.

The imaginary part of the QNM,  $\omega_{\text{im}}^{\text{EEH}}$ , increases as  $Q_e$  augments; for the gravitational RN-BH it increases as well and decreases after a maximum at  $Q/M = 0.9$ . Shown in Fig. 5 is the behavior of the Lyapunov exponent  $\lambda$  from which the imaginary QNM frequencies are calculated,  $\omega_{\text{im}} = |\lambda|/2$  for  $n = 0$ . The two different EM frequencies are compared with those corresponding to the RN-BH. For the RN-BH to have horizons the charge is constrained to  $Q^2 < M^2$ , while the EEH-BH does not have this constraint as a consequence of the screening of the charge. Instead the constraint is  $Q^2/M^2 \leq 25/24$ . The relative magnitudes, for a fixed charge are  $\omega_{\text{im}}^{\text{EEH}_1} > \omega_{\text{im}}^{\text{EEH}_2} > \omega_{\text{im}}^{\text{EEH}_g} > \omega_{\text{im}}^{\text{RN}}$ .

The real part of the QNM is  $\omega_r = l\Omega_c$ , with the orbital angular velocities  $\Omega_c^{(i)}$  (47) given by

$$\begin{aligned}
 M^2 (\Omega_c^{(i)})^2 = & \left( \frac{1}{r^4} [Q_e^2 + r(r-2)] \right. \\
 & \left. \times \left( 1 - 2\mu \frac{a_i Q_e^2}{r^4} \right) - \mu \frac{Q_e^2}{20r^8} \right) \Big|_{r_{ic}}, \quad (50)
 \end{aligned}$$

where  $a_1 = 7$  and  $a_2 = 4$  and we kept the terms up to  $\mathcal{O}(\mu)$  as well. For the analysis of the real part of the QNM, we

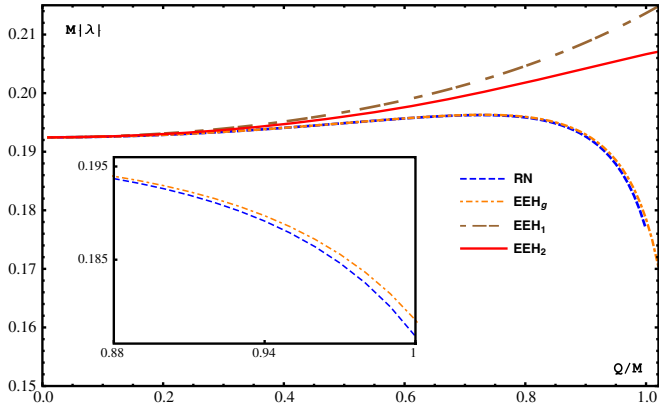


FIG. 5. The behavior of the Lyapunov exponent  $\lambda$  from which the imaginary part of the QNM is obtained, shown as a function of  $Q/M$  for the electric EEH-BH and RN-BH.  $\omega_{\text{im}}^{\text{EEH}} = |\lambda|/2$  increases as  $Q_e$  augments; the same tendency follows RN-BH QNM but these decrease after a maximum at  $Q/M = 0.9$ . The relation  $\omega_{\text{im}}^{\text{EEH}} > \omega_{\text{im}}^{\text{RN}}$  implies a shorter time for the damping of the perturbations in the EEH-BH as compared with the RN-BH. Also shown is the fundamental mode  $n = 0$ , and  $\mu/M^2 = 0.5$ .

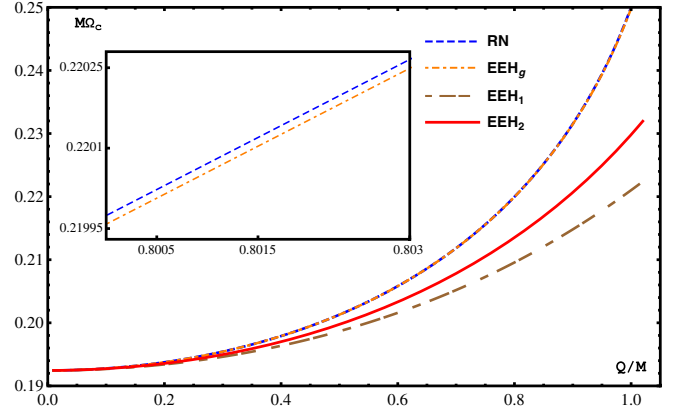


FIG. 6. The behavior of the real part of the QNM, normalized to  $l$ ,  $\omega_r/l = \Omega_c$  as functions of  $Q_e$  for the EEH-BH and RN-BH perturbations shown. The RN angular velocity is almost indistinguishable from the angular velocity for the EEH gravitational perturbations ( $\text{EEH}_g$ ). In the small box we see that the EEH-BH gravitational perturbations have a smaller velocity than the RN, while the electromagnetic angular velocities are smaller than the gravitational ones. The EH parameter  $\mu$  is fixed to  $\mu/M^2 = 0.5$ .

consider  $\omega_r/l \rightarrow \omega_r$ . In Fig. 6 the behavior of the angular velocity or the real QNM frequencies  $\omega_r/l$  of the EEH-BH for values of  $Q_e$  in the range  $0 \leq Q_e^2/M^2 \leq 25/24$  is shown and compared with the RN-BH.  $\omega_r^{\text{EEH}}$  approaches those corresponding to RN as  $Q_e$  decreases. Increasing the charge  $Q_e$  makes  $\omega_r$  increase; the relative magnitudes of the real frequencies are  $\omega_r^{\text{Schw}} < \omega_r^{\text{EEH}_1} < \omega_r^{\text{EEH}_2} < \omega_r^{\text{EEH}_g} < \omega_r^{\text{RN}}$ . Then the gravitational perturbations present slower oscillations than the electromagnetic ones, and the latter are slower than the RN ones, while the slowest are Schwarzschild's ( $Q_e = 0$ ).

From the expressions for  $G_1^e$  and  $G_2^e$  in Eq. (25) we see they depend linearly on the EH parameter  $\mu$ ; the effect of increasing the EH parameter  $\mu$  is increasing the charge screening. In its turn the effect of increasing  $\mu$  on the QNM is enhancing the imaginary part while suppressing the real one.

From the two possible trajectories for light rays in the vicinity of the EEH-BH arise two QNMs, as we have described above, and, in principle, if light were polarized there would be an observable difference in their QNMs. In the case of unpolarized light impinging on the EEH-BH, the EM light trajectory would be obtained by taking an average over the two polarization modes [3,27]. At the present state of the observational facilities, most likely the difference between the two trajectories would be still unnoticeable. Shown in Fig. 7 are the real and imaginary parts of the QNM, varying the charge in a range of  $0.01 < Q_e^2/M^2 < 25/24$  and  $\mu/M^2 = 0.5$ .

#### D. Relaxation times of the EEH-BH perturbations

Another important aspect of the QNMs is their relation with the relaxation times  $\tau$ , that are defined as the inverse of the imaginary part of the QNM,

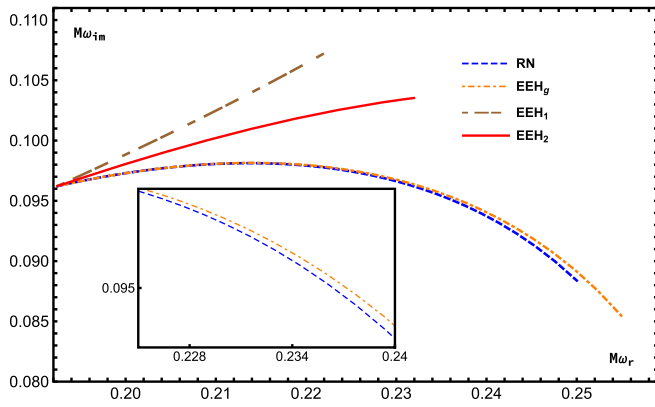


FIG. 7. The behavior of the real and imaginary parts of the EEH-BH perturbations in the eikonal limit is compared with the RN behavior, varying the charge in the range  $0.01 < Q_e^2/M^2 < 25/24$  and fixing  $\mu/M^2 = 0.5$ . They correspond to the fundamental mode  $n = 0$  and the real frequency is normalized with the angular momentum  $\omega_r/l$ .

$$\tau_n = \frac{1}{(n + 1/2)|\lambda|}. \quad (51)$$

In Fig. 8 we compare the relaxation times for the  $n = 0$  mode of the gravitational and electromagnetic perturbations of the EEH-BH and the ones of the RN-BH. It is clear that the effect of the EH-NLED is to diminish the relaxation times as compared with the RN-BH, implying then that the EEH system recovers the stationary state faster than the RN-BH for any of the perturbations, gravitational or

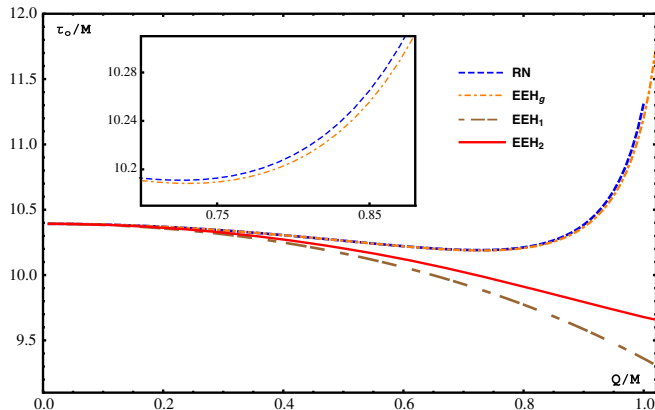


FIG. 8. The relaxation times for the gravitational ( $EEH_g$ ) and electromagnetic perturbations ( $EEH_1, EEH_2$ ) of the EEH-BH are compared with those corresponding to the RN-BH. For small charges,  $\tau_0^{EEH_g}$  and  $\tau_0^{RN}$  go hand in hand (see small box); we find that  $\tau_0^{EEH_g} < \tau_0^{RN} < \tau_0^{Schw}$  for charges  $Q_e < 0.9$ . However when  $Q$  approaches its upper bound ( $Q_e/M$  should be less than 1 for the RN-BH to have horizon) the relaxation time grows, giving then a longer life to the gravitational and RN perturbations. In contrast, the electromagnetic EEH-BH perturbations are always decreasing as  $Q$  augments. In this plot  $\mu/M^2 = 0.5$  and  $n = 0$ .

electromagnetic. Comparing the relaxation times for the gravitational (or massless scalar) perturbations with the RNs,  $\tau_{0g}^{EH}$  and  $\tau_0^{RN}$  go hand in hand. We find that  $\tau_{0g}^{EH} < \tau_0^{RN}$  and  $\tau_0^{RN} < \tau_0^{Sch}$  for charges  $Q < 0.9$ ; however, when  $Q$  approaches its upper bound ( $Q_e/M$  should be less than 1 for the RN-BH to have horizon) the relaxation time grows, giving then a longer life to perturbations. In contrast, the electromagnetic EEH-BH perturbations are always decreasing as  $Q$  augments.

### E. Temporal evolution of the EEH-BH perturbations

Regarding the temporal evolution of the perturbations to the EEH-BH our educated guess is based on the interpretation of the EH field effect as the screening of the charge. In [36] it was shown that for an RN-BH scalar, perturbations are a prototype for all others—electromagnetic, gravitational and higher spin—and it was proved that scalar perturbations radiate completely away, but they die more slowly the larger the BH electric charge. Taking into account the screening charge effect, this leads us to infer that, for a fixed electric charge, the EEH-BH perturbations have a shorter life compared to the linear counterpart RN-BH; this applies to both gravitational and EM perturbations and to every angular momentum  $l$ .

## VI. CONCLUSIONS

In Euler–Heisenberg nonlinear electrodynamics the birefringence effect occurs in such a way that there are two effective optical metrics whose null geodesics are the light trajectories, and following one or the other depends on light polarization. Effective optical metrics are obtained from the background metric and the NLED energy-momentum tensor. In this case the background metric is the EEH–BH metric and the energy momentum tensor is the Euler–Heisenberg. We have determined the two effective metrics followed by photons for both the electric and the magnetically charged EEH-BH.

As an application of birefringence we have calculated the QNM frequencies, in the eikonal limit, of the electromagnetic perturbations of the EEH-BH. These QNM frequencies were calculated from the two possible null unstable geodesics of the effective optical metrics. From the expressions of the real and imaginary parts of the QNM frequencies,  $\omega_{QNM} = \omega_r - i\omega_{im} = \Omega_c l - i(n + \frac{1}{2})|\lambda|$ , and Eqs. (46) and (47), it is clear that the NLEM effects will modify the QNM frequencies by enhancing the imaginary part  $\omega_{im}$  and suppressing the real one  $\omega_r$ ; this effect comes from modifying the metric factors, electric  $G_i^e$  or magnetic  $G_i^m$ ,  $i = 1, 2$ , in the effective metrics [Eqs. (25) and (29)].

The comparison is then done with the QNM frequencies of the Maxwell linear counterpart, the RN–BH. As can be observed in Fig. 5 for the Lyapunov exponent and in Fig. 6 for the angular velocity, the NLEM effect of increasing the electric charge  $Q_e$  is of enhancing the imaginary part

while suppressing the real one, i.e., relaxation occurs faster and oscillation periods are shorter. The magnetic case, the corresponding QNM that we do not explore in detail, follows the same tendencies as the electric case. This can be asserted from the expressions for the Lyapunov exponent and the angular velocity, Eqs. (46) and (47), since the magnetic factor  $G_i^m$  appears inversely to the electric  $G_i^e$  one, but  $G_i^e > 1$  while  $G_i^m < 1$ ,  $i = 1, 2$ . We addressed as well the gravitational perturbations of the EEH-BH, calculated from the null geodesics of the background metric; these perturbations go hand in hand with those corresponding to the RN-BH, with the difference being so slight as shown in the small boxes of the corresponding graphics. On the other hand, the effect of the EH parameter  $\mu$  is of screening the electric charge that renders a more Schwarzschild-like behavior in general, while the effect on the QNM is such that when  $\mu$  increases the imaginary part of the QNM continues increasing, pointing to a shorter time for restoring the unperturbed

state of the EEH-BH as compared to the linear case of the RN-BH. The opposite tendency occurs with the real part of the QNM frequencies,  $\omega_r$ , that is suppressed as  $\mu$  increases. Additionally, we comment on the relaxation times that are shorter than the ones of the linear case; as for the temporary evolution of the perturbations, they die faster for a given charge than the ones of the RN-BH. Finally we can mention that a thorough analysis is needed to know how the modifications introduced by NLEM effects influence the BH stability. Steps in this direction were taken, for instance, in [32] for an NLED Lagrangian  $\mathcal{L}(F)$ .

## ACKNOWLEDGMENTS

N. B. acknowledges partial financial support from CONACYT-Mexico through Project No. 284489. The authors acknowledge financial support from SNI-CONACYT, Mexico.

- 
- [1] T. Gold, Rotating neutron stars as the origin of the pulsating radio sources, *Nature (London)* **218**, 731 (1968).
  - [2] M. G. Baring, Photon splitting and pair conversion in strong magnetic fields, *AIP Conf. Proc.* **1051**, 53 (2008).
  - [3] Z. Bialynicka-Birula and I. Bialynicki-Birula, Nonlinear effects in quantum electrodynamics. photon propagation and photon splitting in an external field, *Phys. Rev. D* **2**, 2341 (1970).
  - [4] E. Brezin and C. Itzykson, Polarization phenomena in vacuum nonlinear electrodynamics, *Phys. Rev. D* **3**, 618 (1971).
  - [5] C. de Melo, L. Medeiros, and P. Pompeia, Causal structure and birefringence in nonlinear electrodynamics, *Mod. Phys. Lett. A* **30**, 1550025 (2015).
  - [6] A. N. Luiten and J. C. Petersen, Detection of vacuum birefringence with intense laser pulses, *Phys. Lett. A* **330**, 429 (2004).
  - [7] H. Gies, Strong laser fields as a probe for fundamental physics, *Eur. Phys. J. D* **55**, 311 (2009).
  - [8] F. Karbstein, Probing vacuum polarization effects with high-intensity lasers, *Particles* **3**, 39 (2020).
  - [9] G. Brodin, M. Marklund, and L. Stenflo, Detection of QED Vacuum Nonlinearities in Maxwell's Equations by the Use of Waveguides, *Phys. Rev. Lett.* **87**, 171801 (2001).
  - [10] H. Euler and B. Kockel, The scattering of light by light in the Dirac theory, *Naturwissenschaften* **23**, 246 (1935).
  - [11] W. Heisenberg and H. Euler, Folgerungen aus der Dirac'schen theorie des positrons, *Z. Phys.* **98**, 714 (1936); English translation: Consequences of Dirac's theory of positrons, *Z. Phys.* **98**, 714 (1936).
  - [12] V. Ferrari and B. Mashhoon, New approach to the quasinormal modes of a black hole, *Phys. Rev. D* **30**, 295 (1984).
  - [13] V. Cardoso, A. S. Miranda, E. Berti, H. Witek, and T. V. Zanchin, Geodesic stability, Lyapunov exponents and quasinormal modes, *Phys. Rev. D* **79**, 064016 (2009).
  - [14] S. Alarcon Gutierrez, A. L. Dudley, and J. F. Plebanski, Signals and discontinuities in general relativistic nonlinear electrodynamics, *J. Math. Phys. (N.Y.)* **22**, 2835 (1981).
  - [15] V. A. De Lorenci, R. Klippert, M. Novello, and J. M. Salim, Light propagation in nonlinear electrodynamics, *Phys. Lett. B* **482**, 134 (2000).
  - [16] R. Ruffini, Yuan-Bin Wu, and She-Sheng Xue, Einstein-Euler-Heisenberg theory and charged black holes, *Phys. Rev. D* **88**, 085004 (2013).
  - [17] D. Amaro and A. Macías, Geodesic structure of the Euler-Heisenberg static black hole, *Phys. Rev. D* **102**, 104054 (2020).
  - [18] S. Gunasekaran, D. Kubiznák, and R. B. Mann, Extended phase space thermodynamics for charged and rotating black holes and Born-Infeld vacuum polarization, *J. High Energy Phys.* **12** (2012) 110.
  - [19] S. I. Kruglov, On generalized Born-Infeld electrodynamics, *J. Phys. A* **43**, 375402 (2010).
  - [20] B. Toshmatov, Z. Stuchlík, and B. Ahmedov, Rotating black hole solutions with quintessential energy, *Eur. Phys. J. Plus* **132**, 98 (2017).
  - [21] M. Guerrero and D. Rubiera-Garcia, Nonsingular black holes in nonlinear gravity coupled to Euler-Heisenberg electrodynamics, *Phys. Lett. B* **788**, 446 (2019).
  - [22] S. I. Kruglov, Remarks on Heisenberg-Euler-type electrodynamics, *Mod. Phys. Lett. A* **32**, 1750092 (2017).
  - [23] N. Breton, C. Lämmerzahl, and A. Macías, Rotating black holes in the Einstein-Euler-Heisenberg theory, *Classical Quantum Gravity* **36**, 235022 (2019).

- [24] H. Yajima and T. Tamaki, Black hole solutions in Euler-Heisenberg theory, *Phys. Rev. D* **63**, 064007 (2001).
- [25] Y. N. Obukhov and G. F. Rubilar, Fresnel analysis of wave propagation in nonlinear electrodynamics, *Phys. Rev. D* **66**, 024042 (2002).
- [26] E. Goulart and S. E. Perez Bergliaffa, A classification of the effective metric in nonlinear electrodynamics, *Classical Quantum Gravity* **26**, 135015 (2009).
- [27] M. Novello, V. A. De Lorenci, J. M. Salim, and R. Klippert, Geometrical aspects of light propagation in nonlinear electrodynamics, *Phys. Rev. D* **61**, 045001 (2000).
- [28] S. Liberati, S. Sonego, and M. Visser, Scharnhorst effect at oblique incidence, *Phys. Rev. D* **63**, 085003 (2001).
- [29] S. I. Kruglov, Nonlinear electrodynamics with birefringence, *Phys. Lett. A* **379**, 623 (2015).
- [30] N. Breton and L. A. Lopez, Quasinormal modes of nonlinear electromagnetic black holes from unstable null geodesics, *Phys. Rev. D* **94**, 104008 (2016).
- [31] R. A. Konoplya and Z. Stuchlik, Are eikonal quasinormal modes linked to the unstable circular null geodesics?, *Phys. Lett. B* **771**, 597 (2017).
- [32] E. Chaverra, J. C. Degollado, C. Moreno, and O. Sarbach, Black holes in nonlinear electrodynamics: Quasinormal spectra and parity splitting, *Phys. Rev. D* **93**, 123013 (2016).
- [33] B. Toshmatov, Z. Stuchlik, J. Schee, and B. Ahmedov, Electromagnetic perturbations of black holes in general relativity coupled to nonlinear electrodynamics, *Phys. Rev. D* **97**, 084058 (2018).
- [34] B. Toshmatov, Z. Stuchlik, and B. Ahmedov, Electromagnetic perturbations of black holes in general relativity coupled to nonlinear electrodynamics: Polar perturbations, *Phys. Rev. D* **98**, 085021 (2018).
- [35] B. Toshmatov, Z. Stuchlik, B. Ahmedov, and D. Malafarina, Relaxations of perturbations of spacetimes in general relativity coupled to nonlinear electrodynamics, *Phys. Rev. D* **99**, 064043 (2019).
- [36] J. Bičák, Gravitational collapse with charge and small asymmetries. II. Interacting electromagnetic and gravitational perturbations, *Gen. Relativ. Gravit.* **12**, 195 (1980).